Transient regime in nonlinear transport through many-level quantum dots

Valeriu Moldoveanu,[1] Vidar Gudmundsson,[2] and Andrei Manolescu[1]
[1]*National Institute of Materials Physics, P.O. Box MG-7, Bucharest-Magurele, Romania*
[2]*Science Institute, University of Iceland, Dunhaga 3, IS-107 Reykjavik, Iceland*
(Received 7 March 2007; revised manuscript received 4 July 2007; published 17 August 2007)

We investigate nonstationary electronic transport in noninteracting nanostructures driven by a finite bias and time-dependent signals applied at their contacts to the leads. The systems are modeled by a tight-binding Hamiltonian, and the transient currents are computed from the nonequilibrium Green-Keldysh formalism. The numerical implementation is not restricted to weak coupling to the leads and does not imply the wideband limit assumption for the spectral width of the leads. As an application of the method we study in detail the transient behavior and the charge dynamics in single and double quantum dots connected to leads by a steplike potential, but the method allows as well consideration of nonperiodic potentials or short pulses. We show that when the higher-energy levels of the isolated system are located within the bias window of the leads, the transient current approaches the steady state in a nonoscillatory smooth fashion. At moderate coupling to the leads and fixed bias the transient acquires a steplike structure, the length of the steps increasing with system size. The number of levels inside a finite bias window can be tuned by a constant gate potential. We find also that the transient behavior depends on the specific way of coupling the leads to the mesoscopic system.

DOI: 10.1103/PhysRevB.76.085330 PACS number(s): 73.23.Hk, 85.35.Ds, 85.35.Be, 73.21.La

I. INTRODUCTION

The dynamics of conduction electrons in open nanostructures modulated by time-dependent signals is an outstanding problem in quantum transport theory. Extensive experimental and theoretical work has been done especially on quantum pumping[1–6] (a detailed bibliography can be found in Ref. 7) and photon-assisted tunneling (see Ref. 8 and references therein). In these phenomena one is interested in measuring or computing the current response of a mesoscopic system driven by time-dependent *periodic* signals applied either on the system or on the attached leads. In particular, an unbiased system subjected to two periodic potentials differing by a phase lag generates a nonvanishing pumped current, provided one averages over the relevant period.[4] If the signal frequency is small, the pumping is adiabatic and can be described by a "frozen" scattering matrix as is rigorously shown in Ref. 9. A photon-assisted tunneling implies instead high frequencies and the measured current displays satellite peaks due to the additional sidebands.[10]

From the theoretical point of view, any calculation of the current starts from defining the initial equilibrium state of the system and the perturbation that drives it. One way is to start with the connected system in the absence of the bias and then to apply the bias adiabatically, performing linear response calculations for the steady-state current. An alternative picture was proposed by Caroli *et al.*,[11] which takes as the equilibrium state the state of the decoupled system with the bias already imposed on the leads. The perturbation here is instead the coupling to the leads that is usually adiabatically switched in the remote past and eventually reaches its full magnitude at $t=0$. If one assumes that a steady state is achieved, the Green functions depend only on time differences and the Keldysh formalism gives the corresponding current in terms of Fourier-transformed quantities. Both pictures were shown to be useful in capturing and explaining important effects.

As for an ac signal, it can be included in the Green-Keldysh approach as a time-dependent global shift of the spectrum of the leads.[12] Note that the occupation probability (i.e., the Fermi function) of the leads stays time independent. Therefore this procedure assumes somehow that an ac signal is applied as well adiabatically. In the quantum pumping calculations the pumping potential is applied to the system in a steady state, be it subjected to a finite bias or not. Finally the current (transient, time averaged, or steady state) is computed from the Keldysh-Green function formalism.[13]

Here we aim to get some insight into a related topic: the calculation of the transient current through a quantum dot (QD) whose coupling to the leads is time dependent while the bias applied to the leads is constant. There are considerably fewer theoretical results on this issue (see the references below), and we were motivated also by recent increasing interest in using suitable electric pulses to investigate relaxation processes in quantum dots by using pump and probe measurements or transient current spectroscopy.[14] As in the well-known case of a turnstile pump[15] these techniques imply oscillating tunnel barriers so that the transport formalism should deal with the nonlocal time-dependent coupling between the leads and the system.

The problem we want to look at is defined as follows: (i) The system is disconnected at any time $t<0$, and the leads are submitted to a constant bias which is included through the difference between the chemical potentials of the leads. (ii) At $t=0$ the leads are *suddenly* plugged to the system. Physically this means that the tunneling barriers between the leads and the system are set to be very high at $t<0$ and drop suddenly at $t=0$ to an intermediate value that allows charge transfer across the system. The simplest case of a constant barrier height at any $t>0$ opens already the problem of the existence of nonequilibrium steady states in the long-time limit. In general and at a rigorous level, one can prove the existence of such states when $t\to\infty$,[16] and moreover, a Landauer formula was shown to hold for the steady-state current.[17] The method we developed is able to check the

passage from transient behavior to the steady-state regime for specific systems, like many-level one- and two-dimensional quantum dots. As we shall see, the onset of the steady state for a given system depends on its structure (number of levels), on the measurement setup (the strength of the coupling to the leads and the location of the contacts), and also on external parameters like gate potentials.

Although in the present work the numerical simulations are restricted to the steplike coupling to the leads, our model allows consideration of more general time-dependent potentials between the leads and the central region. In particular we can investigate the response of a system to *nonlocal* time-dependent perturbations that can be switched on and off individually.

Recently there have been several theoretical approaches to the transient regime. In Ref. 18 the time-dependent density functional was used to compute the transient current in a one-dimensional system submitted to a finite bias applied on the leads. The coupling term does not depend on time, and the system is in an equilibrium state in the absence of the bias. Starting from this state the Kohn-Sham equation is used to calculate the response of the system to the external bias. The same techniques allow the calculation of time-averaged current in one-dimensional quantum pumps.[19] On the other hand, Maciejko and co-workers[20] have computed within the Keldysh framework the response of a single-site dot for a steplike or periodic signal applied to the *leads*, beyond the wideband limit. In their approach the computation of the time-dependent Green functions of the perturbed system uses steady-state Green functions of the coupled and biased system that have to be provided from density functional theory. We believe that theoretical results regarding the transient regime induced by time-dependent couplings of many-level systems would complement these results.

The content of the paper is organized as follows: Section II presents the model and the theoretical tools we use to compute the transient current. We rely essentially on the nonequilibrium Green-Keldysh formalism. However, in contrast to most of the previous studies we allow a complex structure for the central region coupled to leads (i.e., there is more than one single localized level and the system can be as complicated as we want: a single dot, a double dot, or an Aharonov-Bohm interferometer). Also we go beyond the wideband limit approximation and we solve exactly the integral Dyson equation for the retarded Green function of the *coupled* central region by a suitable numerical procedure. In doing so we take into account *all* the scattering processes between the leads and the sample.

Although the electron-electron interaction could presumably play an important role in the transient behavior and the formalism we use allows the inclusion of Coulomb terms in the Hamiltonian, we do not take it into account in this work. As is well known, the problem of the Coulomb interaction in the Keldysh approach is mainly technical and implies suitable approximation schemes for the interaction self-energy. We discuss the validity of our approach and possible ways to include the electron-electron interaction at the end of Sec. II. Section III gives an extensive discussion of the numerical simulations for single and double dots. Section IV concludes the paper.

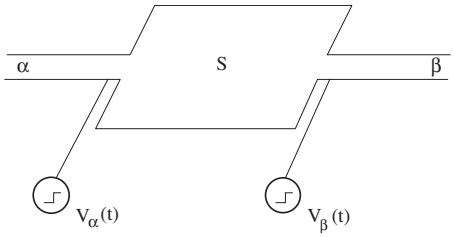

FIG. 1. Schematic picture of the system. The steplike potential is applied between the leads and the central region S at $t=0$.

II. FORMALISM

The systems we study in this work have a typical transport configuration: a central region (S) coupled to two semiinfinite leads (α and β) via a tunneling term (see Fig. 1 for a schematical representation). We shall use a tight-binding (TB) description of the Hamiltonian which has the following form:

$$H(t) = H_S + H_L + H_T(t), \tag{1}$$

where H_S describes the system, H_L is the semiinfinite leads, and $H_T(t)$ is the time-dependent tunneling term:

$$H_T(t) = \sum_{\gamma=\alpha,\beta} \sum_{i\in\gamma} \sum_{m\in S} V_{im}(t)(c_i^\dagger d_m + \text{H.c.}). \tag{2}$$

Here c_i and $c_i^\dagger$ denote the annihilation and creation operators on the ith site of the lead γ. Similarly d_m and $d_m^\dagger$ are the pair of operators corresponding to the mth site from the central region S. $V_{im}(t)$ is the time-dependent hopping coefficient between the ith site of the lead γ and the mth site of the central region. We take here a nearest-neighbor coupling so the double sums in the above expression contain only pairs of sites from the leads end point and the corresponding contact region from the central system:

$$V_{im}(t) = \begin{cases} V_\gamma(t), & \text{if } i,m \text{ nearest neighbors,} \\ 0, & \text{otherwise.} \end{cases} \tag{3}$$

In this work we consider a steplike potential—i.e., $V_\gamma(t) = V_\gamma$ if $t>0$ and zero otherwise. H_S has a usual tight-binding form

$$H_S = \sum_{m=1}^{N} (\epsilon_m + V_g) d_m^\dagger d_m + \sum_{\langle m,n\rangle} t_{mn} d_m^\dagger d_n. \tag{4}$$

Here t_{mn} are hopping terms and $\langle m,n\rangle$ denotes nearest-neighbor summation over the system sites. ϵ_m is the on-site energy, and the diagonal term V_g simulates a plunger gate potential applied on the system. N is the number of sites in the central region. The spectral width of the tight-binding lead is as usual $w := [-2t_L, 2t_L]$, where t_L is the hopping energy of the leads (we take the same hopping constant in every lead). In the numerical calculation we choose t_L such that it covers entirely the spectrum of the central region but we do *not* assume it to be infinite, as is done in the wideband limit approximation.

The central problem in electronic transport is to compute the statistical average of the time-dependent current operator

in a given lead (say, α), $J_\alpha(t)=\mathrm{Tr}\{\rho(t)j_\alpha(t)\}$, using the statistical operator $\rho(t)$. Notice that the time dependence of the current operator appears only because of the time-dependent coupling. Denoting by $\{i_\alpha\}$ the end-point sites of the lead α which are coupled to the sites $\{m_\alpha\}$ of the central region and by M the number of sites in the transverse direction of the lead, the operator j_α that gives the current flowing from the lead α towards the sample has the form (we take the electron charge as $-e$ and $e>0$)

$$j_\alpha(t)=\frac{ie}{\hbar}\sum_{i_\alpha=1}^{M}\sum_{m_\alpha\in C_\alpha}V_{i_\alpha m_\alpha}(t)(c_{i_\alpha}^\dagger d_{m_\alpha}-d_{m_\alpha}^\dagger c_{i_\alpha}). \tag{5}$$

Since the statistical operator $\rho(t)$ of the coupled system is not easy to compute, it is useful to move the time dependence entirely to the current operator by writing $\rho(t)$ in terms of the equilibrium statistical operator ρ_0 of the disconnected system. In general, the coupling to the leads is established at a given instant t_0 so that $\rho(t)=\rho_0$ for $t<t_0$. Then using the unitary evolution $\tilde{U}$ of the full Hamiltonian in the interaction picture with respect to the unperturbed one the solution of the quantum Liouville equation is given by

$$\rho(t)=e^{-it(H_S+H_L)}\tilde{U}(t,t_0)\rho(t_0)\tilde{U}(t,t_0)^*e^{it(H_S+H_L)}. \tag{6}$$

Then it can be shown (see, e.g., Ref. 22) that

$$J_\alpha(t)=\mathrm{Tr}\left\{\rho_0 T_C\left[\exp\left(-i\int_C ds\,\tilde{H}_T(s)\right)\tilde{j}_\alpha(t)\right]\right\}, \tag{7}$$

where T_C is the ordering operator on the Schwinger-Keldysh contour C that runs from t_0 to t and back to t_0. We remind the reader that in the case of adiabatic coupling the statistical operator becomes time independent only in the remote past $t_0\to-\infty$. Both the coupling and current operators are written in the interaction picture. Using the definitions of the lesser Green functions in terms of the Heisenberg operators,

$$G^<_{m_\alpha i_\alpha}(t,t')=i\langle c_{i_\alpha}^\dagger(t')d_{m_\alpha}(t)\rangle,$$

$$G^<_{i_\alpha m_\alpha}(t,t')=i\langle d_{m_\alpha}^\dagger(t')c_{i_\alpha}(t)\rangle, \tag{8}$$

and the fact that they can be equally expressed in terms of operators in the interaction picture [see Eq. (B4) in Ref. 12] it follows that the current is given by a simpler relation

$$J_\alpha(t)=\frac{2e}{\hbar}\sum_{i_\alpha=1}^{M}\sum_{m\in C_\alpha}\mathrm{Re}[V_{i_\alpha m_\alpha}(t)G^<_{m_\alpha i_\alpha}(t,t)]. \tag{9}$$

At this point the standard Keldysh formalism requires the application of the so-called Langreth rules[13] in order to express the lesser Green function $G^<_{m_\alpha i_\alpha}$ in terms of the Green functions of the central region in the presence of the leads, $G^{<,R}_{m_\alpha n_\alpha}$, and the Green functions of the isolated semiinfinite lead, $g^{<,A}_{i_\alpha j_\alpha}$. The latter can be analytically computed:

$$g^A_{i_\alpha j_\alpha}(t,t')=i\theta(t'-t)\sum_{p=1}^{M}\chi_p(i_\alpha)\chi_p(j_\alpha)\times\int_{-2t_L+E_p}^{2t_L+E_p}dE\,\rho(E-E_p)e^{-iE(t-t')}, \tag{10}$$

$$g^<_{i_\alpha j_\alpha}(t,t')=i\sum_{p=1}^{M}\chi_p(i_\alpha)\chi_p(j_\alpha)\times\int_{-2t_L+E_p}^{2t_L+E_p}dE\,\rho(E-E_p)e^{-iE(t-t')}f_\alpha(E). \tag{11}$$

In the above equations $E_p=2t_L\cos[p\pi/(M+1)]$ is the energy of the transverse channel p. These channels appear due to the width of the leads which in the tight-binding description is given by the number of the sites M in the transverse direction. More exactly, the many-channel lead is constructed by taking M semiinfinite one-dimensional (1D) leads and by coupling them through nearest-neighbor hopping constants. Then $\chi_p(i_\alpha)=\sqrt{\frac{2}{M+1}}\sin\left(\frac{pi_\alpha\pi}{M+1}\right)$ is the transversal eigenfunction associated with E_p, and $\rho(E)$ is the density of states at the end point of a semi-infinite one-dimensional lead:

$$\rho(E)=\theta(2t_L-|E|)\frac{\sqrt{4t_L^2-E^2}}{2t_L^2}. \tag{12}$$

Finally, $f_\alpha(E)$ is the Fermi function in the lead α. The bias is included in our approach as the difference between the two chemical potentials of the leads, $V=\mu_L-\mu_R$.

Plugging all these elements in the current formula one gets the main expression that will be numerically implemented in the next section:

$$J_\alpha(t)=-\frac{2e}{h}\mathrm{Im}\left(\sum_{p=1}^{M}\sum_{m_\alpha,n_\alpha\in C_\alpha}\int_{-2t_L+E_p}^{2t_L+E_p}dE\int_0^t ds\,e^{-iE(s-t)}\times\Gamma^{\alpha,p}_{m_\alpha n_\alpha}(E;t,s)[G^R_{m_\alpha n_\alpha}(t,s)f_\alpha(E)+G^<_{m_\alpha n_\alpha}(t,s)]\right). \tag{13}$$

We have introduced the energy and time-dependent quantity $\Gamma^{\alpha,p}_{m,n}$, which takes also into account the M channels in the lead:

$$\Gamma^{\alpha,p}_{m_\alpha n_\alpha}(E;t,s)=\sum_{i_\alpha j_\alpha=1}^{M}\rho(E-E_p)\chi_p(i_\alpha)\chi_p(j_\alpha)V_{i_\alpha m_\alpha}(t)V_{j_\alpha n_\alpha}(s). \tag{14}$$

A similar formula can be written down for the current J_β flowing from the sample β towards the sample. We can therefore define the total charge current

$$J(t)=J_\alpha(t)+J_\beta(t). \tag{15}$$

One should have in mind that the total current is obtained by adding as well the total displacement current $edN(t)/dt$ (see Ref. 23). It is important to observe that in contrast to the simple case of a single-site system the expressions for the

two currents imply Green functions at different contacts. The retarded and lesser Green functions are then to be computed from the Dyson and Keldysh equations.[13]

$$G^R(t,t') = G_0^R(t,t') + \int_0^t dt_1 G^R(t,t_1) \int_0^{t_1} dt_2 \Sigma^R(t_1,t_2) G_0^R(t_2,t'), \tag{16}$$

$$G^<(t,t') = \int_0^t dt_1 G^R(t,t_1) \int_0^{t'} dt_2 \Sigma^<(t_1,t_2) G^A(t_2,t'), \tag{17}$$

where $G_0^{R,A}(t,t')$ are the retarded and advanced Green functions of the isolated central region and $\Sigma^{R,<}$ are the retarded and lesser self-energies. $G_0^R(t,t')$ has a simple expression in terms of the discrete spectrum $\{E_\lambda\}$ of the central region and its localized eigenfunctions ψ_λ (clearly $\lambda=1,\ldots,N$):

$$G_{0,mn}^R(t,t') = -i\theta(t-t') \sum_\lambda \psi_\lambda(m) \overline{\psi_\lambda(n)} e^{iE_\lambda(t-t')}. \tag{18}$$

We emphasize the lower integration limit $t=0$ in Eqs. (16) and (17). This is due to the fact that there is no coupling for $t<0$. In the adiabatic setup the coupling is established in the remote past and one should set a lower cutoff in the numerical implementation. However, the Dyson equation still contains two coupled integrals. The two self-energies above contain information from the leads and are finite rank matrices in the Hilbert space of the central region S ($\gamma=\alpha,\beta$):

$$\Sigma_{mn}^R(t,t') = \sum_\gamma V_\gamma(t) g_{i_\gamma j_\gamma}^R(t,t') V_\gamma(t') \delta_{mm_\gamma} \delta_{nn_\gamma}, \tag{19}$$

$$\Sigma_{mn}^<(t,t') = \sum_\gamma V_\gamma(t) g_{i_\gamma j_\gamma}^<(t,t') V_\gamma(t') \delta_{mm_\gamma} \delta_{nn_\gamma}. \tag{20}$$

We stress that the indices of the leads' Green function are unambiguously determined as the neighbor sites of the contact surface C_α. In the single-channel case $M=1$ one recovers simpler expressions. In particular the retarded Green function of the lead can be expressed through the Bessel function of the first kind:

$$g_{1_\gamma 1_\gamma}^R(t,t') = \frac{-i\theta(t-t')J_1[2t_L(t-t')]}{2t_L(t-t')}. \tag{21}$$

We point out the difference between the exact form of the retarded self-energy and the simple wideband limit expression [which simplifies to $\delta(t-t')$ up to some constants]. Note that the retarded Green function gives the leads' self-energy and is a highly oscillating function. It will turn out in Sec. III that this behavior has crucial effects on the transient current. Another difficulty of Eq. (16) comes from the quadratic dependence of the self-energies on the time-dependent coupling. Clearly this prevents any partial Fourier transform trick.

Given these, our strategy in solving the integral Dyson equation relies on transforming it into an algebraic equation of the form $AX=B$ where A,X,B are generalized complex matrices depending on both spatial and time arguments. To this end we first plug the retarded self energy from Eq. (19) into the Dyson equation (16) and discretize the time arguments. Note that the variable t_2 is defined on a denser grid than the one used for t_1. The inner time integral is evaluated by a repeated four-point Gauss method, which turned out to be accurate enough for the numerical results to be stable when increasing the number of integration steps. This procedure allows us to write the double integral as a matrix $\tilde{G}^R\tilde{A}$, where $\tilde{A}$ is actually a product of G_0^R,Σ^R and some diagonal matrices containing the Gauss weights needed in the integration procedure. Then the adjoint of the generalized retarded Green function $\tilde{G}^R$ is simply the solution of the algebraic equation $(1-\tilde{A})^*\tilde{G}^{R*}=\tilde{G}_0^{R*}$. The true Green function is recovered by turning back the mixed indices of $\tilde{G}^R$. We stress that by solving the equation for $\tilde{G}^{R*}$ the Dyson equation is solved exactly. Moreover, no matrix inversion is required. This is certainly an advantage in the numerical simulations since it is known that matrix inversion is both memory and time consuming. The advanced Green function is computed using the identity $G_{ij}^A(t,t')=(G_{ji}^R(t',t))^*$ and the lesser Green function is derived from the Keldysh equation. Also, the time-dependent occupation number can be computed as

$$N(t) = \mathrm{Im} \sum_{m\in S} G_{mm}^<(t,t). \tag{22}$$

The current in the right lead, J_β, has a similar expression. We note that for a system with many sites one has to deal with different contact Green functions besides replacing only the Fermi function in the first term in the current formula. Moreover, in the nonstationary regime the current obeys the continuity equation $J_\alpha+J_\beta=-edN(t)/dt$. Therefore the steady-state identity $J_\alpha=-J_\beta$ is recovered when the occupation number in the system becomes a constant. We shall discuss this feature below.

In the Keldysh approach to time-dependent transport the problem is to extract physical information from the two contributions in Eq. (13). In the simplest case of a single site and within the wideband limit it was shown that the *average* current obeys a Landauer-like formula. The effects of step-like or harmonic time-dependent potentials applied adiabatically to the leads were studied both in the WBL approach[12] and beyond.[20] However, to our best knowledge no transient current calculation for a many-level structure beyond the wideband limit has been performed within the Keldysh formalism.

Before presenting the numerical results we would like to make some comments concerning the noninteracting approach taken in this work and possible extensions. The electron-electron interactions are known to be important especially in weakly coupled quantum dot systems due to the Coulomb blockade effect. Therefore our results are more accurate at moderate or large coupling to the leads (most of the plots shown in Sec. III correspond to this case). On the other hand, by neglecting the electron-electron interactions our present calculation cannot fully capture the effect of the induced displacement currents (see Ref. 23). The displacement current is defined as the variation of charge accumulated in

the system. As we shall see in the next section, the occupation number of the dot $N(t)$ given in Eq. (22) clearly depends on time in the transient regime and reaches a constant value in the steady-state regime. This shows that our approach takes into account a displacement current though it is a noninteracting one. In spite of this we believe that the features we found in the transient behavior of many-level dots are qualitatively correct, even without including the electron-electron interactions. This is because the transient effects appear mainly due to the back-and-forth processes the electrons experience once the coupling to the noninteracting leads is established; our approach clearly takes all these processes into account. The inclusion of the interaction would only make the transition to the steady state longer as the Coulomb repulsion could lead to a longer time needed to achieve a constant occupation number in the system.

The inclusion of electron-electron interactions in theoretical approaches to time-dependent transport presents some technical difficulties but it is possible in our approach, following three steps: (i) computing the Green functions of the noninteracting coupled system starting from the Green functions of the disconnected subsystems (dot and leads), as shown above; (ii) using these functions, one has then to compute the interaction self-energy in a perturbative framework; and (iii) the interaction self-energy from step (ii) should be introduced then into the corresponding Dyson and Keldysh equations for the full Green functions. In the steady-state regime, such an approach was taken in Ref. 24 in order to describe the controlled dephasing effect. A similar strategy was implemented for ac transport in Kondo regime by Lopez *et al.*[25]

III. NUMERICAL SIMULATIONS

In all the plots the bias, the energy, the hopping constants on the leads, the coupling strengths, and the gate potentials will be expressed in terms of the hopping energy of the central region t_D which is chosen as energy unit. The current is therefore given in units of $et_D/\hbar$ and the time expressed in units of $1/t_D$. Since the spectrum of the two-dimensional discrete Laplacian covers the range $[-4t_D, 4t_D]$, we shall take $t_L=2$ in order to match it to the spectral width of the one-dimensional lead $[-2t_L, 2t_L]$. We take also $e=\hbar=1$. The current given by Eq. (13) can be written as a sum of two contributions

$$J_\alpha(t) = J_\alpha^R(t) + J_\alpha^<(t), \tag{23}$$

the $<$ and R labeling emphasizing that the corresponding term contains the lesser and retarded Green functions. We shall consider for simplicity only single-channel leads.

A. Single site

We start this section by discussing the case of a single-site dot which allows a qualitative discussion of the transient regime and of the transition towards the steady state. The site is coupled to single-channel leads (i.e., $N=M=1$). Both leads are coupled suddenly to the system with the same strength U—i.e., $V_\alpha=V_\beta:=U$. The bias is applied symmetrically to the leads—i.e., $\mu_{\alpha,\beta}=\mu_0\pm eV/2$, μ_0 being the chemical potential of the unbiased leads. We observe that for $\mu_0=0.0$ the single eigenvalue of the isolated system $E_0=0.0$ is located in the middle of the bias window $W=[\mu_0-eV/2, \mu_0+eV/2]$. As we shall see later on, the position of the eigenvalues of the system within the bias window has important implications on the transient current. The free retarded Green function of the single-site system is simply $G_0^R=-i$ but the full retarded Green function is still given by the *integral* Dyson equation and an analytic solution is not at hand.

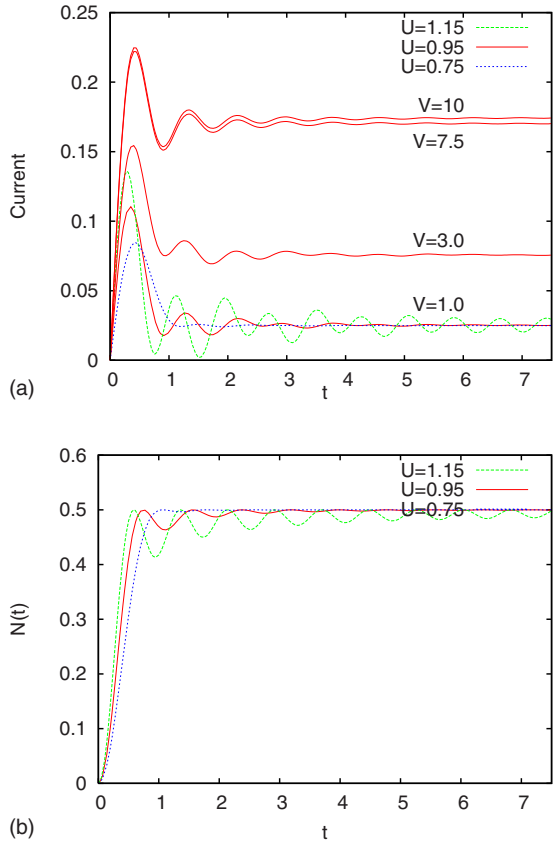

FIG. 2. (Color online) (a) The transient current for one site coupled to single-channel leads. We present curves for different values of the coupling strength U and of the bias V. (b) The effect of the coupling amplitude U on the occupation number. The bias is fixed to $V=1.0$ and $kT=0.0001$.

Figure 2(a) gives the transient current for different values of the bias V and of the coupling amplitude U and reveals that the parameter that controls the shape and the amplitude of the oscillation is the coupling strength U. At moderate coupling $U=0.75$ the steady state (SS) is achieved fast but an oscillatory behavior is observed at $U=0.95$. The case $U=1.15$ is beyond the perturbative regime and the steady state is not achieved in the selected time range. As the bias increases the current saturates for values of V that exceed the spectrum of the leads (i.e., for $V>8$), emphasizing the nonlinear transport regime. In turn, the bias affects neither the amplitude nor the period of the oscillations. This is due to the fact that in our model, as in all approaches based on the Keldysh formalism, there is no term in the Hamiltonian to describe the voltage drop across the sample, the bias being

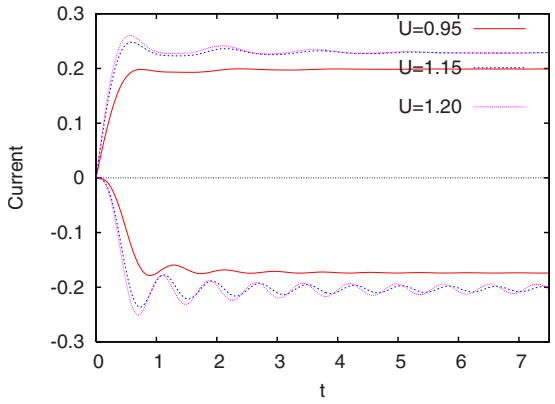

FIG. 3. (Color online) The two contributions to the transient current in the left lead. $J_\alpha^R(t)$ is always positive while the lesser contribution $J_\alpha^<(t)$ is negative. The chosen values for the coupling strength U are given in the figure. The bias $V=1.0$ and $kT=0.0001$.

included only via the Fermi functions of the leads.

In Fig. 2(b) we plot the occupation number of the resonant site $N(t)$ for the same parameters as in Fig. 1(a). The behavior with respect to U is similar. A few more things worth to be noticed: (i) In the steady-state regime the occupation of the site is 1/2. (ii) As U increases while the bias stays constant the occupation number reaches its maximum value faster and the value corresponding to the steady state decreases. (iii) Comparing Figs. 2(a) and 2(b) it can be seen that there is no clear relation between the principal maximum of the current and the one of the occupation number; in fact, the electrons are accumulating in the system even after the current starts to decrease towards the steady state.

Figure 3 shows the two contributions to the current J_α^R and $J_\alpha^<$ for $V=1.0$ and several coupling constants considered in Fig. 2. A physical significance of these two currents was proposed in Ref. 12 for the single site case. Although both Green functions at the contacts appearing in the current formula are "dressed" by the leads' self-energy, one could view J_α^R as the current flowing towards the sample and $J_\alpha^<(t)$ as the current from the sample to the lead α. One notices that the currents have opposite signs. Another observation is that the lesser contribution is responsible for the total current oscillations since J_α^R saturates quickly. However, at small times J_α^R grows faster than $J_\alpha^<$, leading thus to a fast increase of the transient.

In order to understand the nature of the oscillations in the transient current and their dependence on the coupling strength U it is useful to rewrite the current formula, Eq. (13), in a more useful form (since we consider a single-site system, there is only one contact site and the indices of the Green functions can be omitted)

$$J_\alpha(t) = -2U^2 \,\mathrm{Im} \int_0^t ds[G^R(t,s)F_1(s,t) + G^<(t,s)F_2(s,t)], \tag{24}$$

where F_1, F_2 are two oscillating integrals:

$$F_1(s,t) = \int_{-2t_L}^{2t_L} dE\, f_\alpha(E)\rho(E)e^{-iE(s-t)}, \tag{25}$$

$$F_2(s,t) = \int_{-2t_L}^{2t_L} dE\, \rho(E)e^{-iE(s-t)}. \tag{26}$$

One can easily observe that actually $F_2(s,t)$ can be expressed through Bessel function of the first kind:

$$F_2(s,t) = \frac{\theta(t-s)J_1[2t_L(t-s)]}{2t_L(t-s)}. \tag{27}$$

For fixed t, F_2 is an oscillating function of s whose oscillation amplitudes increase with s. F_1 does not have a simple analytical expression but it has a similar behavior.

The oscillatory behavior of the current is clearly decided by the convolution in Eq. (24). Besides the oscillations of F_1 and F_2 one expects as well a complex behavior of the Green functions. We recall that the Dyson equation counts the infinite back-and-forth tunneling processes involving the leads and that the amplitudes of these events are even powers of U. Now, the higher-order terms in the Dyson equation contain multiple integrals of products of the leads' self-energy which is highly oscillating [see Eq. (21)] Therefore, if $U \ll 1$, there will be only a few low-order significant contributions from the complicated lead-sample scattering. The critical value $U=1.00$ corresponds to the onset of the nonperturbative regime, and the method we use for solving the Dyson equation captures as well this situation, taken into account all contributions.

We give in Fig. 4 the 3D plots of the imaginary parts for the retarded and lesser Green functions at coupling strength $U=1.20$, which leads to oscillations of the transient. These are the relevant quantities in the current formula since it turns out that the real part of G^R and of F_2 are vanishingly small (not shown).

One observes that $G^R(t,s)=0$ for $s \geq t$ and, more interestingly, that $G^R(t,s)$ and $G^<(t,s)$ exhibit pronounced oscillations as time varies and reach a limit value as s approaches t. In the case of the retarded Green function this limit is *constant* and equals $-i$, which is simply the value of the unperturbed retarded Green function. This feature is easy to understand by looking at the Dyson equation and noticing that when $s \to t$ the integration range of the inner integral shrinks considerably so that at almost equal times the perturbed Green function resembles the unperturbed one. This argument is not restricted to the single-site case we are discussing. Also, since the spectrum of the discrete Laplacian is symmetric, the unperturbed retarded Green function will always be real and therefore the real part of the full Green function will always be vanishingly small, as we shall check numerically in the many site case. In contrast, the limit of $\mathrm{Im}\, G^<$ as $s \to t$ is *not* a constant with respect to t but shows oscillations that disappear as t increases. In the particular single-site case the limit value of $G^<$ is clearly the occupation number of the site, whose oscillations were shown already in Fig. 2(b).

Figures 5(a) and 5(b) show 3D maps of the imaginary part of the lesser Green function and emphasize the role of the

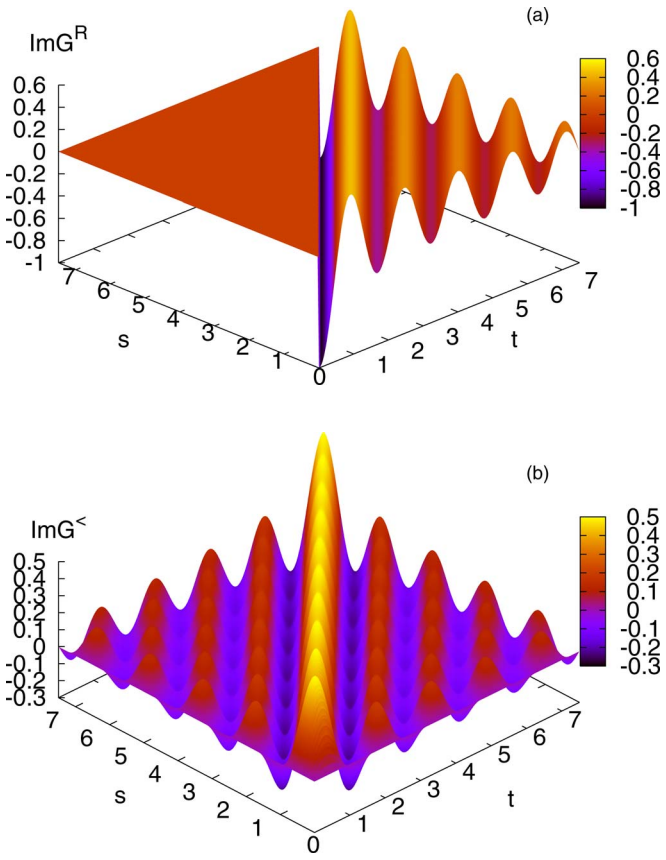

FIG. 4. (Color online) The imaginary parts of the retarded (a) and lesser (b) two-time Green functions of the coupled single site. The bias $V=1.0$ and the coupling strength $U=1.2$. The oscillations seen along the "diagonal" in (b) corresponding to almost equal times are responsible for the oscillations of the occupation number.

coupling strength on the transient. At moderate coupling $U=0.75$ one observes small amplitude oscillations except for $s\sim t$, in clear contrast to the case $U=1.20$ where pronounced oscillations exist even for large time differences. Inspecting the real part of the function F_2 given in Fig. 5(c) we see that it does not depend on t when $s\sim t$ and that this gives the main contribution to the integral (24). It is now clear from Figs. 5(a) and 5(c) that the corresponding current will be nearly stationary once the sample is charged (i.e., for $t>0.75$), because by increasing t the "off-diagonal" contributions are very small (some cancelations being possible as well). When U increases the integral will collect instead nonnegligible contributions from the entire range $(0,t)$ and therefore the current will oscillate. These observations lead to the following statement: The steady state will be achieved at instant t_s if for any $t>t_s$ there are no contributions for long-time differences—i.e., when both contact Green functions $G^R(t,s)$ and $G^<(t,s)$ vanish for $s<t_s$. It is easy to observe that this condition implies the well-known criteria for the steady state $G(t,s)=G(t-s,0)$.

B. Many-site case

We consider now the more interesting case where the central region has more than one level. Figure 6(a) emphasizes

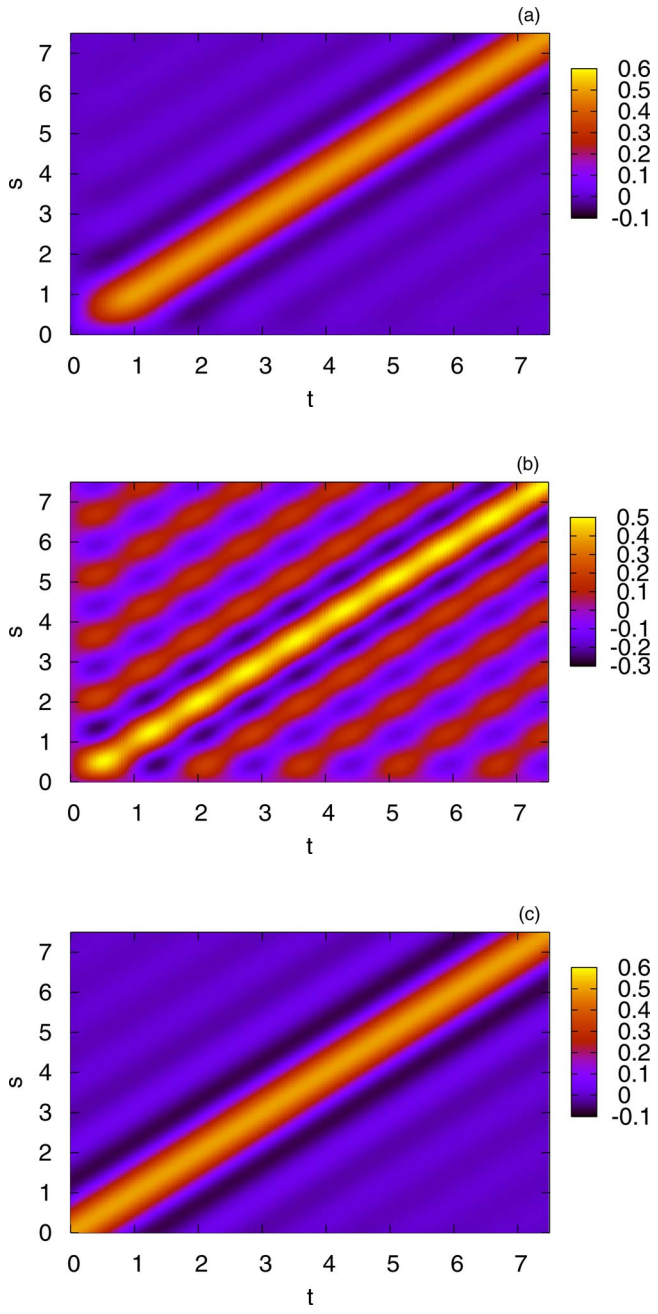

FIG. 5. (Color online) The imaginary part of the lesser two-time Green function for the moderate coupling $U=0.75$ (a) and strong coupling $U=1.2$ (b). (c) The real part of the oscillating function F_2. The bias $V=1.0$.

the qualitative differences between the transients of 1D systems with $N=2,4,6,8$ sites. A general feature is that as the size increases the transient develops a "shoulder" which is not met in the single site case. For $N=2$ a second smaller slope of decrease is noticed for $t\in[1.6:2.5]$. For $N=4$ the system experiences few very different regimes before reaching the steady state. It first decreases faster up to $t\sim 1.25$. For a short time a small hill develops around $t\sim 2$; then, the decrease continues but clearly at a smaller rate. Finally, for $t>3.25$ the current approaches the steady state very slowly. A similar behavior is observed for $N=6$ and $N=8$, the main

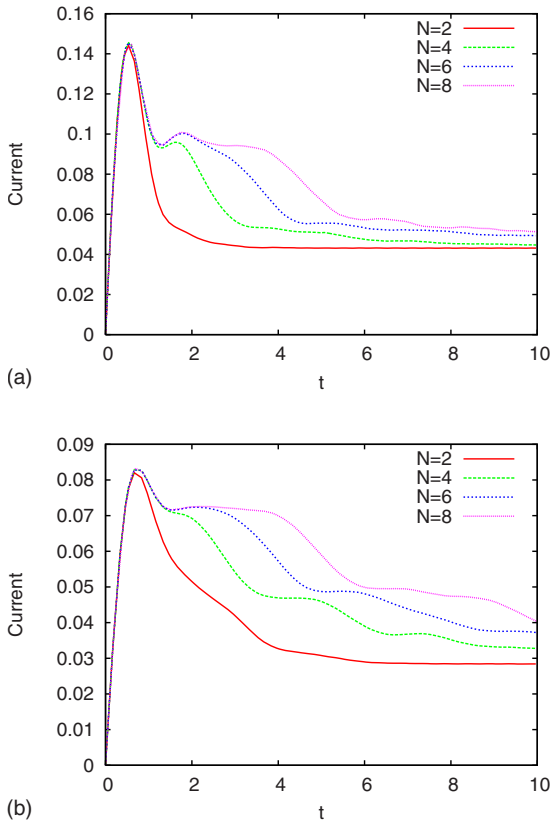

FIG. 6. (Color online) (a) The transient current in the left lead $J_\alpha(t)$ for different sizes of the 1D central region. The number of sites, N, is indicated in the figure. In (a) the coupling to the leads is $U=0.75$ and in (b) $U=0.50$. By decreasing U the shoulders in (a) turn to clear steps in (b). The bias is fixed to $V=2.0$ and $kT=0.0001$.

difference being that the shoulder is longer and the intermediate slope is smaller. The patterns described above suggest that there are some intermediate regimes, some of them being characterized by a rather stable current. Figure 6(b) emphasizes that at lower coupling $U=0.50$ the transient is even smoother and for $N=4,6$, and 8 one notices the formation of clear steps.

When the coupling strength U is increased the transient shows oscillations but they are fewer than in the single site (not shown). Since the two oscillatory integrals over energy in the current formula and both self-energies do not depend on the number of sites in the system, the above size effects should be explained only by the behavior of the contact Green functions. We show in Fig. 7(a) and 7(b) the imaginary parts of the the contact Green functions $G_{11}^{R,<}$ of the four-site system for a strong coupling $U=1.25$ (it turns out again that the real part of G_{11}^R is vanishingly small). Comparing with Fig. 4 it is obvious that for the four-site dot the Green functions have a more regular behavior and in particular the occupation number of the contact site 1 shows milder oscillations than the occupation number of the single site. Figure 7(c) gives the Im $G_{11}^R(t_1=10,t_2)$ as a function of t_2 for different couplings and reveals that at weak coupling to the leads the full retarded Green function is close to the unperturbed one and the electron dynamics inside the system must

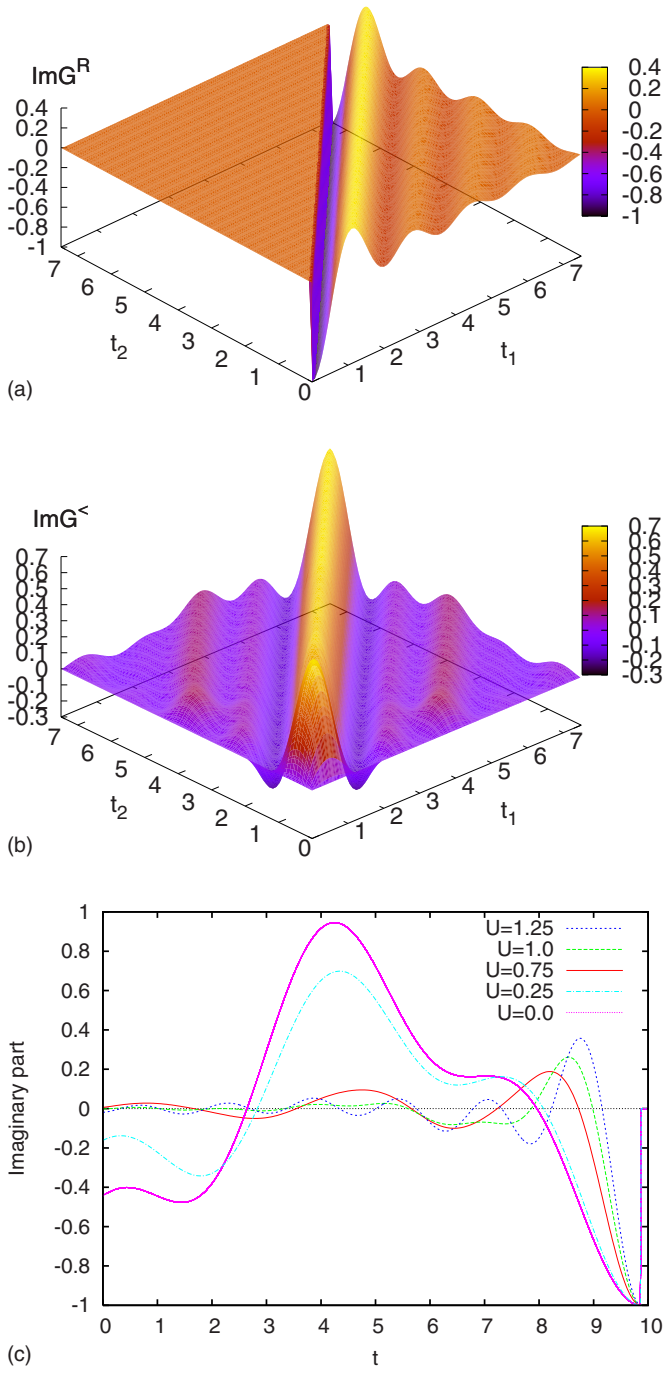

FIG. 7. (Color online) The imaginary part of the left-contact retarded Green function (a) and of the lesser Green function for the four-site system (b). (c) The imaginary part of $G_{11}^R(t_1=10,t_2)$ at different couplings U. At small coupling Im G^R resembles the retarded Green function of the isolated system (the curve corresponding to $U=0.0$).

resemble the one of the isolated sample. Indeed, the curve at $U=0.25$ follows the oscillations of the free Green function which is also given in the figure (the curve corresponding to $U=0.0$). We plot the imaginary part since it turns out again that the real part is vanishingly small, so it does not contribute considerably to the retarded current. As U increases the

Green function changes and shows clear oscillations imposed by the leads' self-energy.

The analysis performed so far has focused on the behavior of the transient current as the intrinsic parameters of the system (i.e., its size and the height of the tunneling barriers at the contacts) are varied. Nevertheless, in a typical transport experiment these parameters are fixed and one usually measures the current by varying the bias or a plunger gate voltage. From steady-state current measurements it is well known that the role of such a gate potential is to bring one or more levels of the quantum dot within the bias window (BW). We show in what follows that at fixed bias and given coupling strength to the leads one can tune the transient current with a gate potential. Moreover, by inspecting the transient behavior as the gate potential is varied, it is possible to extract some information about the number of states within the bias window or above it. We will make the discussion for the four-site dot. The gate potential is simulated by the diagonal term V_g added to the on-site energy of the system. We fix the bias window to $W=2.0$, and for convenience we set $\mu_R=0.0$. Figure 8(a) gives families of transients for coupling strength $U=0.75$ and various values of V_g specified in the figures. Figure 8(b) shows the four levels of the isolated quantum dot as the gate potential scans the range $[-4:4]$. The V_g values chosen in Fig. 8(a) correspond to different locations of the levels with respect to BW. The bottom curve is irregular and settles down to a vanishing current because in this case there is no level within the BW. We note, however, that a nonvanishing transient current still develops shortly after the coupling is established. At $V_g=-1.0$ the highest level is located in the BW and the transient is smooth and already shows the additional shoulder noticed previously. The same thing happens when two states lie in the BW (at $V_g=0.0$), the difference being that the steady-state current increases considerably. For $V_g>0.50$ it is clear from the structure of the spectrum that one cannot have more than two states in the BW and that the levels pass gradually above it. We found it interesting to look at the transient currents for those gate potentials that still allow two states in the transmission range while pushing one or two states above BW. One notices that for $V_g=1.0$ the steady-state currents do not distinguish the different spectral structure involved in transport, while the transient current is very sensitive to it.

In the case of the six-site QD the shoulder in Fig. 4 is more pronounced because at $V_g=0.0$ there are exactly three states inside the bias window. We want to point out that since we have neglected the Coulomb interaction, our simulations cannot capture the transport through *many-body* excited states of the quantum dot. Tunneling processes involving such states would lead to a minipeak structure of the current maxima as a function of the gate potential applied to the system (see Ref. 26). We can consider, however, that our results should describe qualitatively the transport involving more levels because for small dots the bias required to cover the ground state of N electrons is much higher that the excitation energies.

Now we investigate two more features of the transient regime: the time-dependent charge filling of the central region and possible effects due to different shapes of the

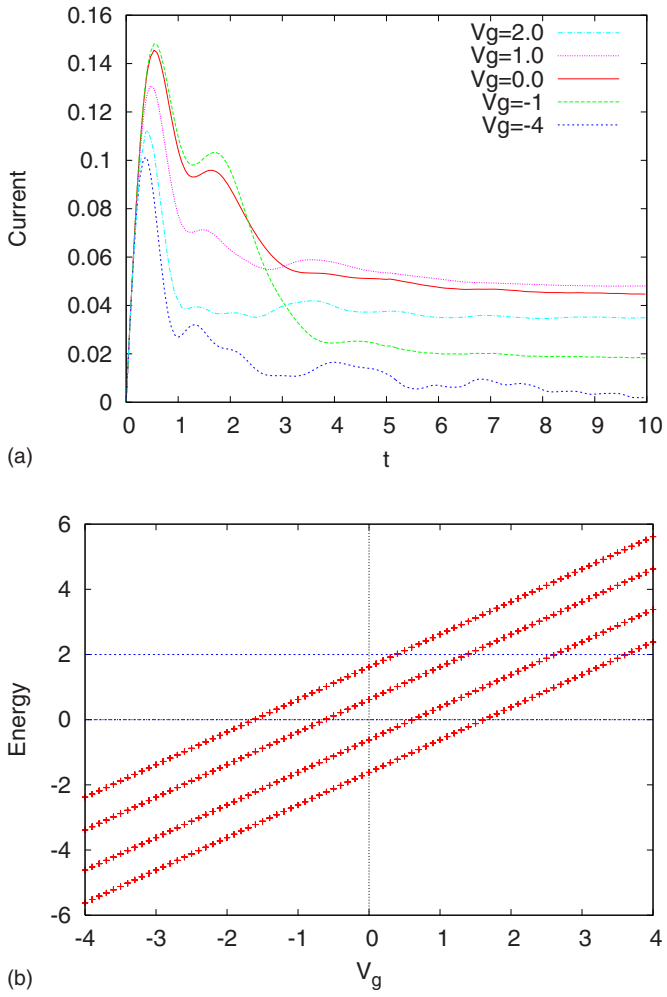

FIG. 8. (Color online) (a) The transient current for different values of the gate potential applied on the four-site quantum dot for $U=0.75$. (b) The spectrum of the system as function of the gate potential. It can be checked that the additional shoulders observed in (a) develop when there is at least one state of the QD in the bias window and no state above it. Other parameters: $V=2$ and $kT=0.0001$. Note that the bias is applied asymmetrically—that is, $\mu_\beta=0.0$.

system or of the various ways in which one can couple the leads. Besides the four-site 1D system discussed so far we consider also a 2×2 quantum dot. Both systems are submitted to the same bias and have equal coupling to the leads. However, in the case of the 2D quantum dot one can use different contacts for plugging the leads. We discuss two situations: (i) a symmetric configuration in which the leads are attached to the opposite corners of the system—namely, at sites 1 and 4—and (ii) an asymmetric coupling when we use the first and third sites as contacts. Figure 9(a) reveals the changes induced in the transient curves in each case. The remaining subfigures show the occupation number $N_i(t)$ of each site $i=1,4$ for the 1D system and the two configurations considered. Inspecting Figs. 9(a) and 9(b) we see that (i) the contact sites 1 and 4 are the first to be populated due to their proximity to leads. (ii) Since $\mu_\alpha>\mu_\beta$, the right-contact site (the fourth) gains less charge at a lower rate than the left-

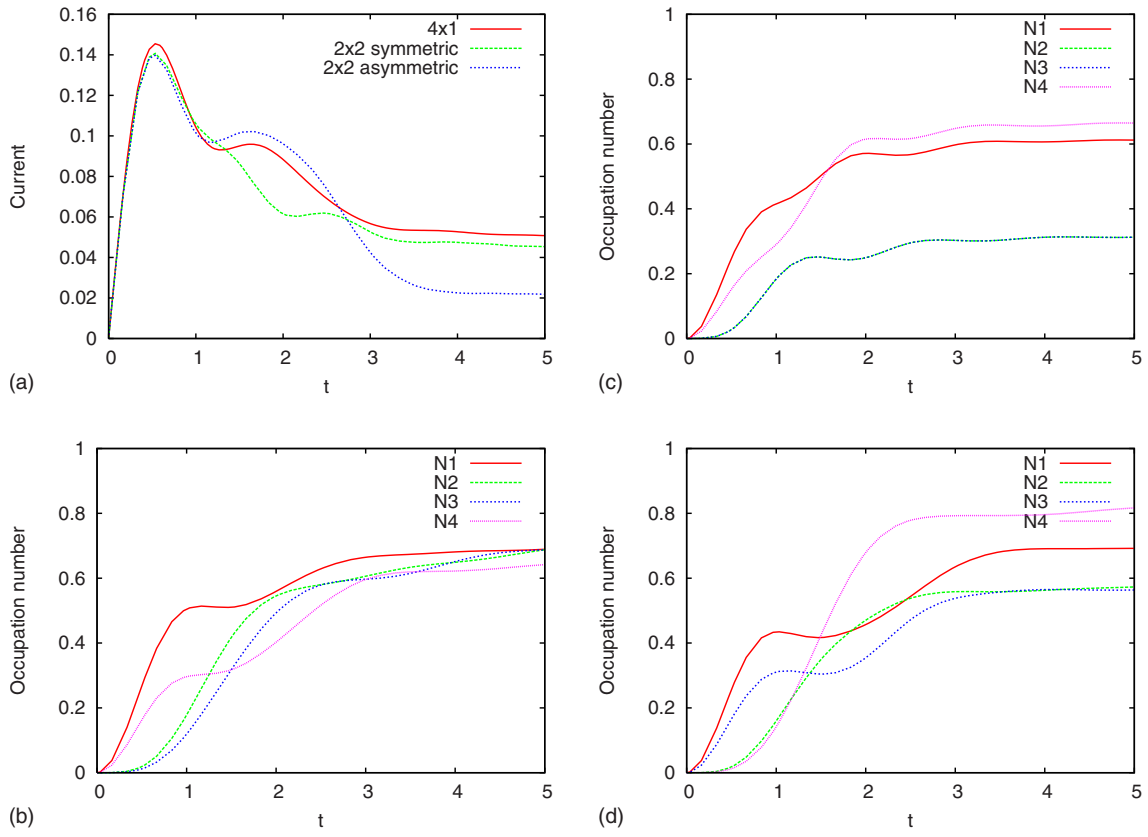

FIG. 9. (Color online) (a) The transient in the left lead $J_\alpha(t)$ for the 4×1 system and for the 2×2 system in the two configurations of the leads as mentioned in the text. (b), (c), (d) The occupation numbers $N_i(t)$ of the ith site for the three cases considered in Fig. 9(a). (b) 1D system, (c) symmetric configuration, and (d) asymmetric. Other parameters: $U=0.75$, $V=2.0$, and $kT=0.0001$.

contact site (the first). Both N_1 and N_4 show a steplike behavior for a short period (around $t=1$). This coincides with the increased occupation number on the middle sites. We note also that the step in the occupation of the contact site N_1 ends when it is equaled by N_2. All sites are then continuously filled up to the steady-state value. The occupation number on the right contact is smaller than the other ones which attain roughly the same value 0.65. (iii) The steplike behavior of the transient currents in the range $[1:1.75]$ corresponds to the almost constant population of the contact sites in the same interval. The symmetric configurations are still characterized by a smooth transient but we notice that the step appears now later that in the 1D case. Figure 9(c) confirms again that this stable regime is assigned to a constant flow in the contact site. Also it reflects the fact that the charge is equally distributed in sites 2 and 3 which are located symmetrically with respect to the leads. In the asymmetric geometry the transient is rather similar to the one of the 1D system up to $t=2.8$ but then drops to a lower steady-state value. The occupation numbers show that the fourth site carries more charge than the contact sites in the steady state. This means in our opinion that part of this charge simply accumulates and is not participating in transport. More interestingly, we note that in contrast to the symmetric geometry N_2 and N_3 are different in the transient regime but reach the same value in the steady state. We mention that time-dependent simulations were performed recently in the case of an Aharonov-Bohm ring starting from the Schrödinger equation.[21]

We discuss now briefly the behavior of the total particle current $J_\alpha+J_\beta$ which is given in Fig. 10 along with its two components (the + sign is due to the fact that the current J_β represents the current from the lead β to the system and therefore has opposite sign). As already mentioned, only in the steady state does one have the identity $J_\alpha=-J_\beta$. Consequently, the net current $J_\alpha+J_\beta$ vanishes. However, in the transient regime the two currents, although having similar shape, differ significantly.

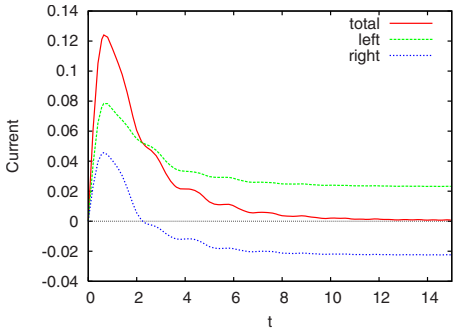

FIG. 10. (Color online) The total transient current and the components in the left lead and right lead. Other parameters: $U=0.5$, $V=2$, and $kT=0.0001$.

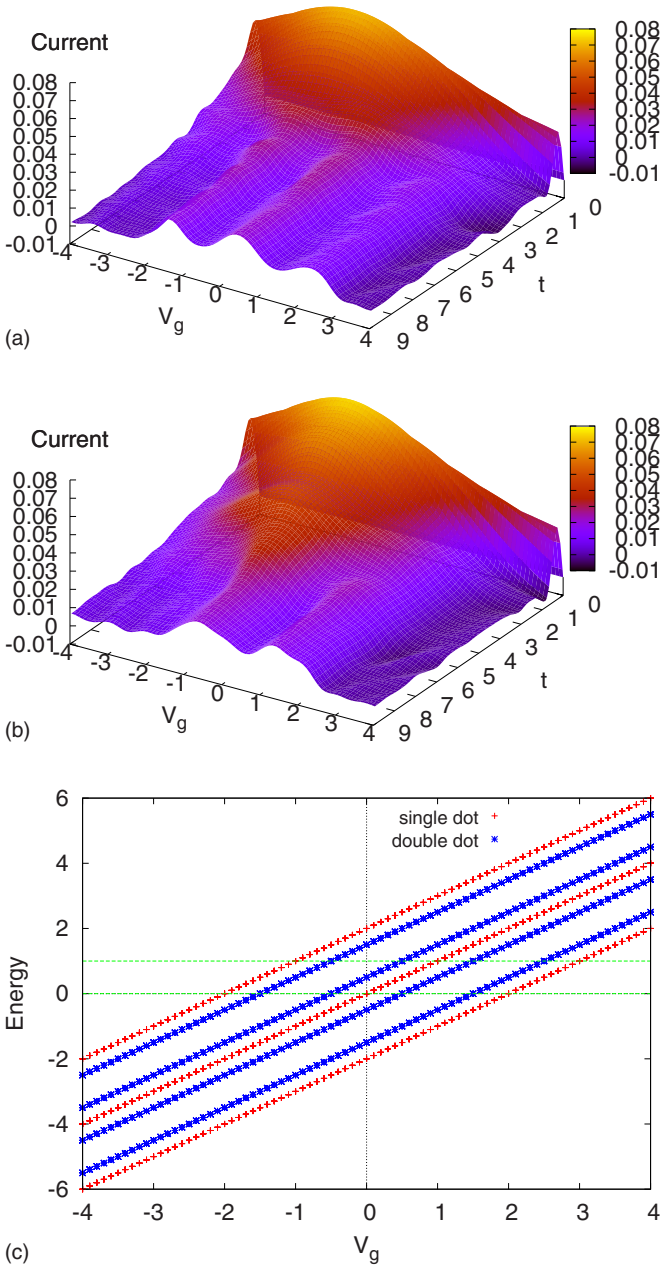

FIG. 11. (Color online) (a) The 3D map of the transient current for a (2×2)-site QD as a function of time and gate potential V_g. The maxima are related to the spectrum of the isolated system given in (c). (b) The 3D map of the transient current for 2×2 the double dot $t_{24}=t_{13}=0.5$. Other parameters: $V=1.0$, $U=0.50$, and $kT=0.0001$. (c) The spectra of the two systems as a function of the gate potential. The lines mark the bias window.

To substantiate further the previous analysis we present in Fig. 11(a) the contour plot of the current as function of time and gate potential for the (2×2) site quantum dot coupled to the leads in the symmetrical configuration. Figure 11(c) gives the spectrum of the system as the gate potential varies. The middle eigenvalue is doubly degenerated. When the levels are either below or above the bias window ($W=1.0$ starting from $\mu_R=0.0$) the transient oscillates for quite a long time before passing to the steady state. We also observe that in these two extreme limits the transient oscillations are qualitatively different. For $V_g\sim-4$ the current shows decreasing oscillations towards the steady state. In contrast, for $V_g\sim4$ one remarks faster oscillations and, more importantly, negative values of the transient. Since in this regime all the levels are above the bias window and there is no way to pass electrons to the right lead, it is clear that the negative current in the left lead is just the reflected one. We underline that this effect is due to the fact that we have considered a finite spectral width of the leads and that similar features were reported for the single-site case.[20] As expected, as the system approaches the stationary regime the current shows three maxima associated with the passage of the localized levels through the bias window. Actually the levels turn to resonances when coupling the leads to the system, but since one has to deal with a time-dependent Hamiltonian, it is difficult to characterize the location and width of these resonances in the transient regime. This is why in the 3D plot one cannot distinguish between different resonances at times $t<3.0$. Figure 11(b) presents the transient current for the same 2×2 system except that the hopping parameters t_{13} and t_{24} are reduced to 0.5. In this case one can view the system as a double dot, each dot composed of two sites. As the spectrum from Fig. 11(b) shows, the degeneracy is lifted and the level spacing diminishes. As a consequence in the long-time regime one gets two broader peaks, since the four levels are now grouped into pairs.

All the features presented above emphasize that the transient regime of the many-level structures is quite different from the single-level system.

IV. CONCLUSIONS

We have performed transient current calculations for a many-level finite system coupled suddenly to semiinfinite biased leads. Our method is based on the nonequilibrium Green-Keldysh machinery. We find numerically an exact solution of the integral Dyson equation which is solved as an algebraic equation. By analyzing the behavior of the retarded and lesser Green functions we explain qualitatively the shape of the transient current and the passage to the steady state. The amplitude of the coupling to the leads controls essentially the convergence to a steady state. We have identified nontrivial effects of the many-level structure of the system and presented an intuitive picture of the charge filling by studying the occupation number inside the system. By increasing the system size the shape of the transient current and the evolution towards the steady state differs significantly from the single-site oscillatory behavior and depends crucially on the number of electronic states available in the bias window. We predict that a steplike structure could be observed in transient current measurements by applying a gate potential on the system that tunes the higher levels within the bias window. Different transients are expected to appear as well when different coupling geometries of the leads are used.

The present method can be used for studying the response of mesoscopic systems to more complicated time-dependent couplings to the leads: pulses having different lengths and decaying rates and nonperiodic signals.

ACKNOWLEDGMENTS

This work was supported in part by the research programme of the Icelandic Research Council for Nanoscience. V.M. was also supported by CEEX Grant No. D11-45/2005. We acknowledge useful discussions with C. S. Tang.

[1] M. Switkes, C. M. Marcus, K. Campman, and A. C. Gossard, Science **283**, 1905 (1999).
[2] L. J. Geerligs, V. F. Anderegg, P. A. M. Holweg, J. E. Mooij, H. Pothier, D. Esteve, C. Urbina, and M. H. Devoret, Phys. Rev. Lett. **64**, 2691 (1990).
[3] P. W. Brouwer, Phys. Rev. B **58**, R10135 (1998).
[4] O. Entin-Wohlman, A. Aharony, and Y. Levinson, Phys. Rev. B **65**, 195411 (2002).
[5] M. Moskalets and M. Büttiker, Phys. Rev. B **66**, 205320 (2002).
[6] L. Arrachea, Phys. Rev. B **72**, 125349 (2005).
[7] L. Arrachea and M. Moskalets, Phys. Rev. B **74**, 245322 (2006).
[8] G. Platero and R. Aguado, Phys. Rep. **395**, 1 (2004).
[9] J. E. Avron, A. Elgart, G. M. Graf, and L. Sadun, Commun. Pure Appl. Math. **57**, 0538 (2004).
[10] W. G. van der Wiel, T. H. Oosterkamp, S. de Franceschi, C. J. P. M. Harmans, and L. P. Kouwenhoven, in *Strongly Correlated Fermions and Bosons in Low-Dimensional Disordered Systems*, edited by I. V. Lerner *et al.* (Kluwer Academic, Dordrecht, 2002), pp. 43–68.
[11] C. Caroli, R. Combescot, P. Nozieres, and D. Saint-James, J. Phys. C **4**, 916 (1971).
[12] A.-P. Jauho, N. S. Wingreen, and Y. Meir, Phys. Rev. B **50**, 5528 (1994).
[13] H. Haug and A.-P. Jauho, *Quantum Kinetics in Transport and Optics of Semiconductors* (Springer, Berlin, 1996).
[14] T. Fujisawa, D. G. Austing, Y. Tokura, Y. Hirayama, and S. Tarucha, J. Phys.: Condens. Matter **15**, R1395 (2003).
[15] L. P. Kouwenhoven, A. T. Johnson, N. C. van der Vaart, C. J. P. M. Harmans, and C. T. Foxon, Phys. Rev. Lett. **67**, 1626 (1991).
[16] W. Aschbacher, V. Jaksic, Yan Pautrat, and C. A. Pillet, in *Lecture Notes in Mathematics*, Vol. 1882, Open Quantum Systems III, edited by S. Attal, A. Joye, and Claude-Alain Pillet (2006), pp. 1–66.
[17] G. Nenciu, J. Math. Phys. **48**, 033302 (2007).
[18] S. Kurth, G. Stefanucci, C.-O. Almbladh, A. Rubio, and E. K. U. Gross, Phys. Rev. B **72**, 035308 (2005); G. Stefanucci and C.-O. Almbladh, *ibid.* **69**, 195318 (2004).
[19] G. Stefanucci, S. Kurth, A. Rubio, and E. K. U. Gross, arXiv:cond-mat/0701279 (unpublished).
[20] Y. Zhu, J. Maciejko, T. Ji, H. Guo, and J. Wang, Phys. Rev. B **71**, 075317 (2005); J. Maciejko, J. Wang, and H. Guo, *ibid.* **74**, 085324 (2006).
[21] B. Szafran and F. M. Peeters, Phys. Rev. B **72**, 165301 (2005).
[22] J. Rammer and H. Smith, Rev. Mod. Phys. **58**, 323 (1986).
[23] B. Wang, J. Wang, and H. Guo, Phys. Rev. Lett. **82**, 398 (1999).
[24] V. Moldoveanu, M. Ţolea, and B. Tanatar, Phys. Rev. B **75**, 045309 (2007).
[25] R. Lopez, R. Aguado, G. Platero, and Carlos Tejedor, Phys. Rev. B **64**, 075319 (2001).
[26] A. T. Johnson, L. P. Kouwenhoven, W. de Jong, N. C. van der Vaart, C. J. P. M. Harmans, and C. T. Foxon, Phys. Rev. Lett. **69**, 1592 (1992).